

See discussions, stats, and author profiles for this publication at: <https://www.researchgate.net/publication/41200466>

Plasmonic Nanoparticle/Polymer Nanocomposites with Enhanced Photocatalytic Antimicrobial Properties

ARTICLE *in* THE JOURNAL OF PHYSICAL CHEMISTRY C · MAY 2009

Impact Factor: 4.77 · DOI: 10.1021/jp901337e · Source: OAI

CITATIONS

45

READS

64

5 AUTHORS, INCLUDING:



Anna Kubacka

Spanish National Research Council

90 PUBLICATIONS 2,218 CITATIONS

[SEE PROFILE](#)



Marta Fernández-García

Spanish National Research Council

160 PUBLICATIONS 2,096 CITATIONS

[SEE PROFILE](#)

Plasmonic Nanoparticle/Polymer Nanocomposites with Enhanced Photocatalytic Antimicrobial Properties

Anna Kubacka,[†] María L. Cerrada,[‡] Cristina Serrano,[‡] Marta Fernández-García,^{*,‡}
Manuel Ferrer,[†] and Marcos Fernández-García^{*,‡}

Instituto de Catálisis y Petroleoquímica, CSIC, C/Marie Curie 2, 28049-Madrid, Spain, and Instituto de Ciencia y Tecnología de Polímeros, CSIC, C/Juan de la Cierva 3, 28006-Madrid, Spain

Received: February 13, 2009; Revised Manuscript Received: April 6, 2009

We present a simple method of fabricating highly efficient antibacterial nanocomposite films consisting of a commercially available ethylene–vinyl alcohol copolymer (EVOH) and embedded Ag–TiO₂ nanoparticles. These systems display potent antimicrobial activity toward Gram-negative, Gram-positive bacteria/cocci (*Escherichia coli* 1337-H; *Pseudomonas putida* KT2440, *Staphylococcus aureus* 1341-H), and yeasts (*Pichia jadini*) and, moreover, show outstanding resistance to biofilm formation. These nanocomposites differ from known and similar TiO₂–EVOH systems by the presence of small quantities (in the 10⁻² wt. % level) of silver. Through a plasmonic effect, the presence of the noble metal significantly enhances the antimicrobial power of TiO₂–EVOH systems upon ultraviolet (UV) light and opens the fruitful use of visible-light excitation sources. A joint UV–visible and photoluminescence optical characterization of the films allows an understanding of the behavior upon both UV and visible light excitations and provides evidence that the biocidal action comes from the inorganic–organic interface and takes place on the whole nanocomposite surface. These properties indicate that the films are potentially useful as antimicrobial materials in a wide variety of packaging, biomedical, and general use applications.

1. Introduction

Modification of polymeric matrices to prevent growth or reduce adhesion of detrimental microorganisms is a highly desired objective. Hence, there is a significant interest in the development of antimicrobial biomaterials for application in the health and biomedical devices, food, and personal hygiene industries.^{1–13} Among several possibilities currently explored, titania (TiO₂) can be spot out as a potential candidate for polymer modification with a significant number of advantages. This oxide is a nontoxic material, even at the nanoscale, widely used in human-related applications,¹⁴ and fulfills the two additional main requirements needed for massive use, wide availability, and modest cost.^{15–17} Moreover, titania displays antimicrobial activity against all kinds of microorganisms, without known weakness in the killing of Gram-positive and negative bacteria, yeast, fungus, and virus.¹⁸ TiO₂ works under UV light excitation with energy above the corresponding band gap (ca. 3.2 eV) forming energy-rich electron–hole pairs. Once at the surface of the material, such charge carriers are able to interact with microorganisms rendering biocidal properties to the corresponding polymer-based nanocomposite films. A point of relevance is the control of the TiO₂ polymorphism ensuring the presence of the anatase form, the one with biocidal capability, as well as to control primary particle size in the nanometer range, a fact that would limit scattering events among other things.^{15–17}

Novel hybrid or nanocomposite organo-inorganic materials that combine attractive qualities of dissimilar oxide and polymer components are not simply physical blends (vide supra) but can be broadly defined as complex materials having both organic

and inorganic constituents intimately mixed. The scale of mixing or, in other words, the degree of homogeneity would influence or even command the properties of the nanocomposite solid materials when the component mixture is adequately reached, typically at the nanometer range.^{19,20} In particular, the optimization of the component contact has been shown to be crucial in order to render TiO₂-containing polymer nanocomposites with outstanding biocidal properties.^{21,22} Another point of importance to improve the performance of TiO₂-containing nanocomposite systems concerns the optimization of light absorption and the adequate handling of subsequent charge (electron–hole) pair creation and annihilation processes. This task has been typically attempted by controlling the morphological-structural-defect characteristics of the oxide and/or by extending its absorption power into the visible region through a doping process.^{15–18} A route to simultaneously influence both light absorption and charge handling is based on the so-called plasmonic photosystems.²³ As detailed above, TiO₂ is excited by near-UV irradiation and a metal such as Ag shows a very intense localized surface plasmon (LSP) absorption band in the near-UV–visible region. Adequate handling of the LPS resonance can allow extending the absorption light into the visible region of the electromagnetic spectrum and, due to the enhancement of the electric near-field in the vicinity of the Ag, would allow boosting the excitation of electron–hole pairs. An overall improvement of the oxide–polymer nanocomposite performance upon excitation on a region ranged from the near-UV (above ca. 280 nm) to the visible light (below ca. 500–525 nm) can be thus envisaged through a plasmonic effect. This would yield highly efficient systems, with improved performance with respect to TiO₂-alone nanocomposites, and having the potential of working under sunlight and/or diffuse artificial light typical of human environments. A last point to mention is the concomitant degradation of the polymer matrix by effect of the charge carriers; this has

* Corresponding authors. E-mail: martafg@ictp.csic.es; mfg@ictp.csic.es.

† Instituto de Catálisis y Petroleoquímica.

‡ Instituto de Ciencia y Tecnología de Polímeros.

been proved to be limited by addition of small amounts of titania, typically below 5 wt. %.^{21,22}

Ethylene–vinyl alcohol copolymer (EVOH)-based composites are described in this work for their application as smart novel materials. A straightforward, cost-effective method was devised to introduce different contents of the inorganic solid into the EVOH polymeric matrix. An optimized 1 wt. % Ag on TiO₂ inorganic component prepared by photodeposition²⁴ was introduced into the polymeric matrix through a melt compounding process without incorporation of coupling agents. Although the system contains Ag (in very low quantities, e.g., below 0.05 wt.%), there is no release of this metal to the medium, as the inorganic component is essentially absent from the surface of the material.²⁵ The method ensures an efficient organo-inorganic contact,²⁵ changing the nature of the inorganic agent and erasing the requirement of a close proximity with the pathogen, making the oxide in the nanocomposite a noncontact agent. To probe this, an extensive screening will be made on biocidal properties of these systems regarding prokaryotic and eukaryotic microorganisms associated to both alimentary and clinical human infections.²⁶ Further, we show the effect on *Pseudomonas putida* KT2440, a paradigm of tolerant microorganism-inhabiting soil, water, plants and animals, able to grow in the presence of high concentrations of extremely toxic and harmful conditions because of its capability to form biofilm.²⁷

2. Experimental Section

Sample Preparation. The TiO₂ component was prepared using a microemulsion synthetic route (characteristic primary particle size below 10 nm).²⁸ Using this material, silver was photodeposited from an aqueous solution of silver nitrate (Merck) to a content of 1 wt. % (metal basis).²⁴ A commercially available ethylene–vinyl alcohol copolymer (EVOH; Solvay), containing a nominal 71 mol-% vinyl alcohol content, was used as polymeric matrix in the preparation of xTiAg (where x stands for the weight percentage of the inorganic component) nanocomposites with different Ag–TiO₂ nanoparticle contents: 0.5, 1, 2, and 5 wt. %. The reference xTi nanocomposites containing exclusively TiO₂ as the inorganic component were previously characterized.²⁵ These novel materials were prepared through melt processing at 195 °C and at 60 rpm for 5 min in an internal mixer with a volumetric capacity of 3 cm³, prototype built in our machine shop scaling from a commercial Haake internal mixer. Previous to this, the nanoparticles and EVOH copolymer were subdued to ultrasonic (Sonics VC505) and stirring cycles to homogenize the batch. After blending and homogenization of these two components, specimens were obtained as films by compression molding in a Collin press between hot plates (210 °C) at a pressure of 1.5 MPa for 5 min. A quench was applied to the different films from the melt to room temperature. Note that the EVOH reference hereafter used is surrendered to the same preparation steps suffered by the nanocomposite materials.

Strains and Bacterial Cultures. The microorganisms used in this study include *E. coli* 1337-H, *P. putida* KT2440, *S. aureus* 1341-H, and *P. jadinii* CECT 1062 and were obtained from the Spanish type Culture Collection (CECT; <http://www.uv.es/cect/>) and the German Collection of Microorganisms and Cell Cultures (DSMZ, Braunschweig, Germany) and cultured and maintained according to the recommendations of the suppliers.²⁹ Cells were grown in 100 mL flasks filled with 10 mL of the respective medium and subsequently used for photochemical cell viability assays. Briefly, *P. putida* KT2440 was at 37 °C grown in minimal medium (MM) prepared as follows. A solution with “Epure”-water containing (NH₄)₂SO₄

(2 g/L), Na₂HPO₄ (6 g/L), KH₂PO₄ (3 g/L), and NaCl (3 g/L) was adjusted to pH 7.0 ± 0.2 and then autoclaved. Afterward the medium was supplemented with 20 mM MgSO₄, 10 μM FeSO₄, and 15 mM Na-benzoate (from a stock solution sterilized by filtration through a 0.22 μm filter (Millipore)). *E. coli* 1337-H and *S. aureus* 1341-H were grown in Luria–Bertani (LB) medium at 37 °C, and *P. jadinii* was cultured in YPD medium containing bacto peptone (10 g/L), yeast extract (10 g/L), and glucose (1% v/v) at 30 °C.³⁰

Photochemical Viability Assays. To study the antimicrobial activity of the films, the overnight cultures were diluted 1:10 in LB, MM, or YPD liquid medium and grown at 30 or 37 °C until the absorbance at 600 nm reached 0.6. Cells were harvested and diluted with broth solution up to ca. 10^{6–8} cfu mL⁻¹. One hundred fifty microliter amounts of these solutions were contacted with the corresponding films under continuous stirring using μCLEAR 96 microtiter plates (Greiner Bio-one). The film-cell slurry was placed in the UV spectrometer array chamber (BioTek Synergy HT) under continuous stirring and irradiated with a UV light of 280 and 500 nm for different periods of time. Care was put of using a sublethal, maximum radiation energy fluence of ca. 1 kJ m⁻² throughout the study.³¹ This was further confirmed with the help of blank tests.

Biofilm Formation Assay. Cells of *P. putida* KT2440 were cultured as described above and used to inoculate 30 mL of prewarmed LB (10 times diluted) to a starting OD₆₀₀ ~ 0.05. One milliliter aliquot samples of this culture was put on the surfaces of interest and incubated stationary at 30 °C for 12 h with or without UV light of 280 nm. Once time elapsed, the cell suspension was removed, and samples were taken, washed three times with 0.1 M 2-(N-morpholino)ethanesulfonic acid (MES) buffer (pH = 7.4) to eliminate any loose or unattached bacteria, and fixed with 2.5% glutaraldehyde (Merck, Darmstadt, Germany) in a 0.1 M MES buffer (pH = 7.4).

Characterization Techniques. Scanning electron microscopy experiments were carried out at room temperature in a XL30 ESEM Philips equipment working at 25 and 15 kV for morphology and microbiology studies, respectively. Samples for morphological analysis were *in situ* cryofractured prior to observations of the film cross-section. The samples were coated with gold–palladium (80:20) with a sputter coater (Polaron SC7640) working at 800 V and 5 mA. Transmission electron microscopy experiments were carried out at room temperature in a 200 kV JEM-2000 FX JEOL microscope. Samples were embedded in Spurr resin (low viscosity epoxy, cured at 60 °C for 48 h) to obtain parallel cuts of the film surface in thin (80 μm) sections by ultramicrotomy (Reichert-Jung Ultracut E), which were picked up on copper grids and coated with a thin layer of carbon graphite (MED 010 Balzers evaporator) to improve heat capacity. The crystal lattice characteristics of the nanocomposites were examined by wide-angle X-ray scattering (WAXS). Patterns were recorded at room temperature in the reflection mode by using a Bruker D8 Advance diffractometer provided with a Goebel mirror and a PSD Vantec detector (from Bruker, Madison, WI) and Cu Kα radiation. The equipment was calibrated with different standards. The diffraction scans were collected at a rate of 1°/min between 2θ values from 4 to 43°. The long spacing determination was performed at room temperature using small-angle X-ray scattering (SAXS) employing synchrotron radiation ($\lambda = 0.150$ nm) at the beamline A2 at HASYLAB (Hamburg, Germany). A MARCCD detector was used for data acquisition, sited at a distance of 265 cm from the sample and calibrated with the different orders of the long spacing of rat-tail cornea ($L = 65$ nm).

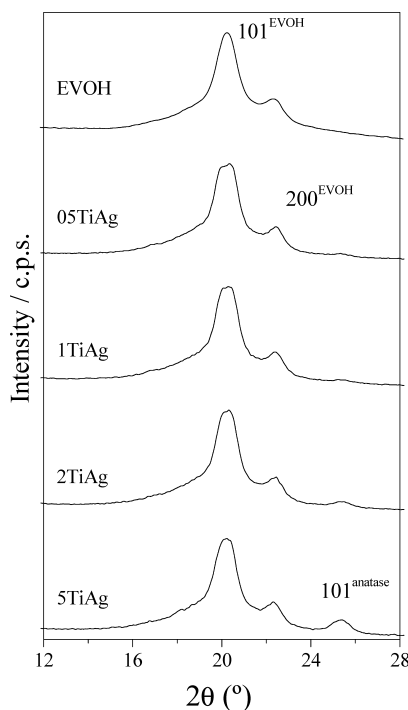


Figure 1. WAXS profiles of the different $x\text{TiAg}$ nanocomposite materials. Diffraction peaks are labeled by their hkl parameters.

Absorption spectra were recorded in transmission with a Cary 6000 from Varian. Raman and photoluminescence measurements were performed at room temperature with LabRAM HR (Horiba) and different laser lines of Ar^+ , Kr^+ (333 nm + 363 nm, and 488 nm) lasers. Spectra are corrected by the instrumental function recorded with a calibrated white source and a CaF_2 pellet.

3. Results and Discussion

The EVOH copolymer is semicrystalline, and WAXS experiments were performed to determine the influence of inorganic nanoparticle incorporation on the crystal lattice developed in the different nanocomposites. Similar WAXS profiles are found at room temperature for all $x\text{TiAg}$ samples and the EVOH polymeric component as depicted in Figure 1. Therefore, all of these $x\text{TiAg}$ quenched specimens show an orthorhombic lattice, without noticeable change with respect to that exhibited by the neat polymeric component. A similar situation was encountered when studying the corresponding $x\text{Ti}$ reference nanocomposites.²⁵ In addition to the rather constant location of the 101 and 200 diffraction peaks characteristic of the EVOH orthorhombic cell,^{32,33} the 101 reflection ascribed to the TiO_2 anatase polymorph (centered at ca. 25° ; JCPDS-84-1286) is seen in the nanocomposites and its intensity increases with the $\text{Ag}-\text{TiO}_2$ content. The crystallinity degree of the different nanocomposites can be estimated from these WAXS patterns by their decomposition into the crystalline diffractions and the amorphous component. The amorphous peak of the different samples was found to be centered at $2\theta = 19.8 \pm 0.1^\circ$. The results reported in Table 1 point out that crystallinity slightly increases by the introduction of the inorganic nanoparticles, although differences are very subtle. Regarding the long spacing also estimated at ambient temperature from the Lorentz-corrected SAXS profiles, it has to be said that a small enlargement is observed as the nanoparticle content raises (see Table 1). Consequently, the most probable crystal size corresponding to the polymeric matrix, determined from the values of long spacing and crystallinity

TABLE 1: Main Physicochemical Characteristics of the Organic Component of $x\text{TiAg}$ and $x\text{Ti}$ Nanocomposites and for the EVOH Copolymer Reference^a

sample	f_c^{WAXS}	L (nm)	l_c (nm)
EVOH	0.39	13.7	5.4
2Ti	0.39	17.0	6.6
0.5TiAg	0.43	15.5	6.7
1TiAg	0.43	16.5	7.1
2TiAg	0.43	17.2	7.4
5TiAg	0.43	17.5	7.5

^a f_c^{WAXS} : crystallinity degree determined by WAXS, L : long spacing estimated by SAXS, and l_c : most probable crystal size. Standard errors (\pm): 7% for f_c^{WAXS} ; 0.5 nm for L and l_c .

assuming a two-phase model, increases slightly with nanoparticle content, although its incorporation does not lead to significant alterations in the crystalline structure of the polymeric matrix.

A SEM/TEM analysis was carried out to study the state of the inorganic component within the nanocomposite films. The cross-section SEM photographs (Figure S1, Supporting Information) showed no microsized aggregated nuclei up to a 5 wt. % of the inorganic component, indicating that inorganic nanoparticles have been highly dispersed within the EVOH matrix and their practical absence at the surface of the material. This behavior parallels the one observed in the $x\text{Ti}$ nanocomposite reference systems.²⁵ The noticeable homogeneity of the $x\text{Ti}$ materials at the nanometer scale has been only possible by tuning the surface/size characteristics of the inorganic nanocomponent. To confirm this aspect, a TEM study of the 2TiAg sample (Figure 2) was performed. In this case, the oxide is dispersed in the polymeric matrix exhibiting nanometer-scale aggregates ranging from 10 (the oxide primary particle size) to 200 nm, with an average size (Feret diameter)³⁴ of 90 nm (± 20 nm). As can be deduced from the high resolution TEM image depicted in Figure 2b, these aggregates are composed of oxide nanoparticles interwoven with the organic component at a nanometer scale. Considering that the titania preparation makes use of an oxide previously calcined at high temperature to ensure the exclusive presence of the anatase polymorph and the strict control of its biocidal capabilities, the nanometric dispersion of the oxide attained in loadings below 5 wt. % is significant, particularly with respect to microsized or bulk titania specimens³⁵ or compared with other inorganic components (clay, SiO_2 , etc.) introduced in polymers.^{36–41} A detailed view of the inorganic–organic interface is presented in Figure 2c. The crystal planes of the inorganic nanoparticles are here well observed together with the more disordered (essentially amorphous according to electron diffraction patterns) polymer matrix surrounding the nanoparticles. The oriented, parallel preferential stacking of both components at interface layers is direct evidence of the perfect match between them in our nanocomposite films.

The large interfacial contact attained in these nanocomposite films reveals unique physicochemical properties, characteristic of the whole system and not of the components. In the context of the biocidal application of polymer-based nanocomposites, the modulation of the optical properties exhibited by the inorganic component is a critical aspect. As mentioned in the introduction, the use of the silver LSP would help in handling light absorption (particularly in the visible range to extend the UV range characteristic of titania) and charge carrier excitation and recombination; both phenomena aimed to positively influence biocidal properties. The UV–visible spectra of the $x\text{TiAg}$ and reference systems are displayed in Figure 3. The EVOH

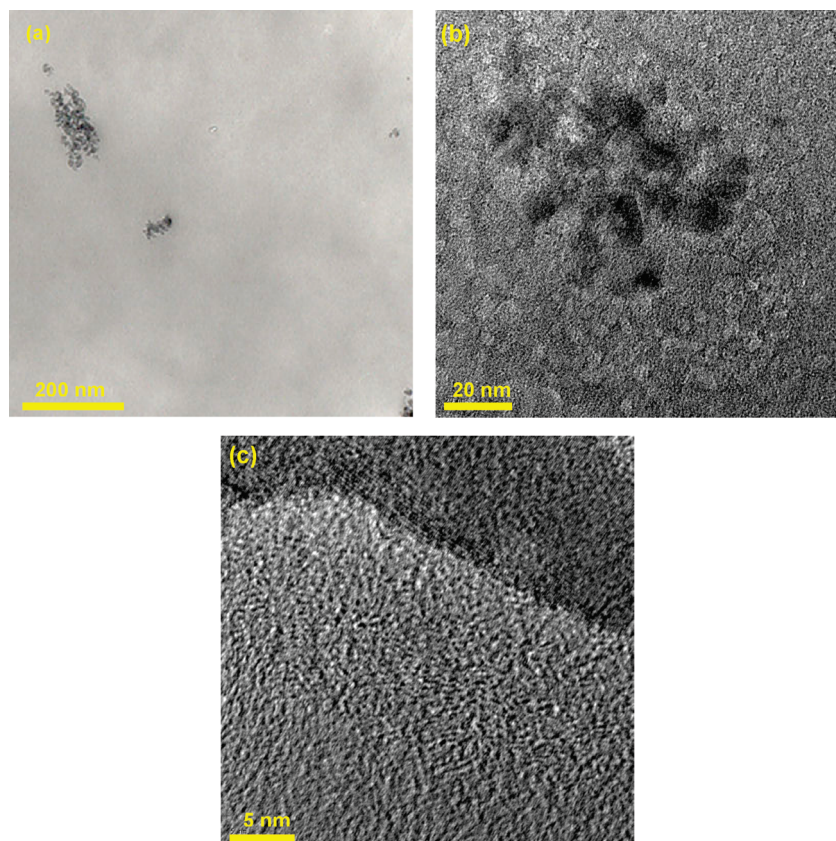


Figure 2. (a) TEM image of the 2TiAg nanocomposite. (b) HR-TEM detail showing a nanometer-scale Ag–TiO₂ aggregate. (c) HR-TEM detail showing a nanometer-scale inorganic–organic interface.

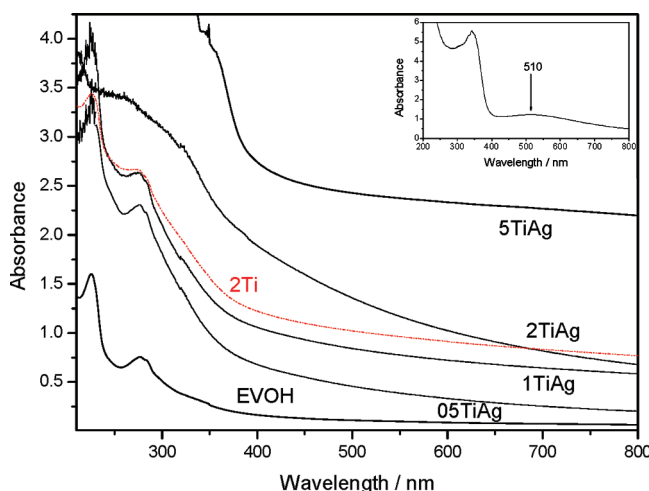


Figure 3. UV–visible absorption spectra of the EVOH component and x TiAg and x Ti nanocomposite materials. Inset shows the spectrum of the TiAg inorganic component.

polymeric component shows a typical insulator behavior with a band gap of ca. 200 nm but also displays localized absorption transitions at ca. 220 and 280 nm ascribed to chromophores existing in the antioxidant additives incorporated because of its industrial nature. Incorporation of the inorganic component to the polymeric matrix produces important changes in the absorption profile. Inorganic nanoparticle loadings below 1 wt. % mainly alter the EVOH spectrum by enhancing the absorbance on the visible region. At 2 wt. % content, changes are more dramatic, and a new, broad absorption feature between 350–500 nm becomes evident. The anatase–TiO₂ band gap is expected at the lower end of this zone (e.g., below 400 nm),^{15–17}

but a comparison with the 2Ti sample indicates the capital role played by the Ag in the enhancement of the absorption in the visible region. The inset of Figure 3 displays the spectrum for the Ag–TiO₂ component used in this series. This shows the presence of the silver LSP resonance at ca. 510 nm, justifying the improvement of the 2TiAg absorbance at the higher wavelength zone within the 350–500 nm range. As previously shown, the plasmon resonance position is characteristic of the binary Ag–TiO₂ system,⁴² differing significantly from the one of isolated, small Ag nanoparticles (below 5 nm).⁴³ The metal–oxide surface interaction and modulation of the metal electronic properties are at the core of this behavior but are poorly understood at the moment. Note that the film silver content is 0.02 wt. % in the 2TiAg material, but this develops rather important absorption features which will be fully interpreted with the help of a photoluminescence study (see below). Finally, the 5TiAg sample shows with clarity the anatase band gap on top of a very high visible-range background absorption level. This energy behavior of the background has been previously reported on other polymer–clay systems and (at least partially) ascribed to an enhancement of light scattering as the number of inorganic centers grows, as a consequence of the nanometric scale (e.g., interference range with UV and visible light) of the inorganic filler.⁴⁴

Photoluminescence (PL) spectra obtained using two excitation energies were thus used to further interpret the optical properties of the nanocomposite systems. Radiative relaxation of such charge carriers can be followed by photoluminescence spectroscopy, which can potentially be used to understand charge handling processes on the whole nanocomposite system.^{45,46} Figure 4 shows the PL spectra of samples excited with visible light (488 nm). Similar spectra are obtained with UV light (result

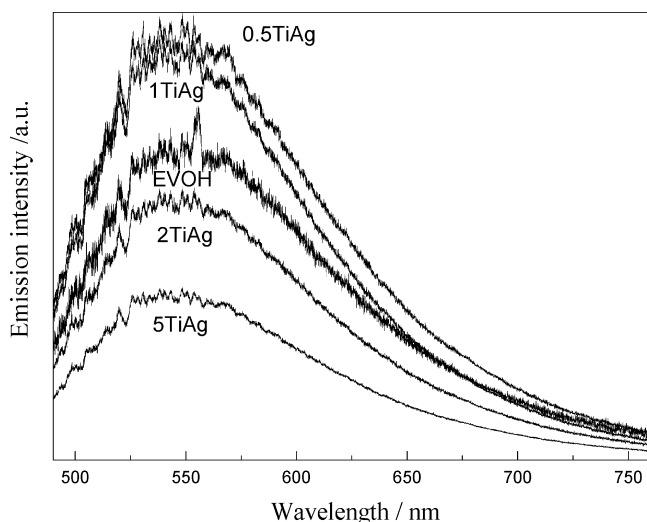


Figure 4. Luminescence spectra of the EVOH component and x TiAg and 2Ti nanocomposites. Excitation line 488 nm (see text for details).

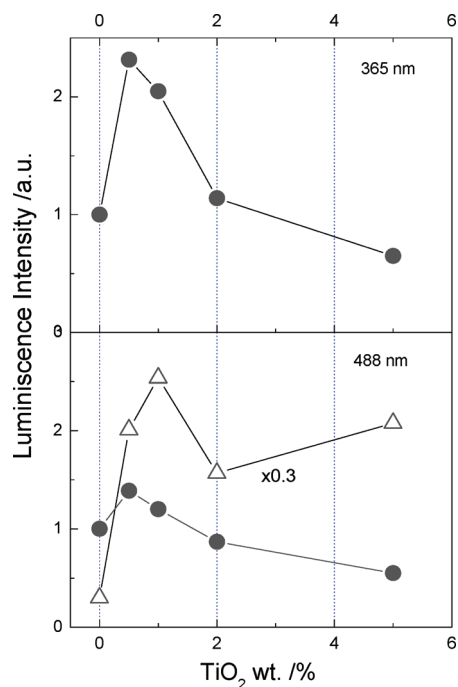


Figure 5. Intensity of the luminescence spectra for the EVOH component and x TiAg nanocomposite materials obtained upon UV-A (333 + 365 nm; top) and visible (488 nm; bottom) excitations (open symbols correspond to reference x Ti nanocomposites).

not shown). Figure 5 depicts the behavior of the PL intensity through the series using UV (365 nm) and visible (488 nm) laser excitations. Note that in the first case, both the EVOH and TiO₂ components can be excited while in the second none of them should be excited. Only the Ag LSP resonance would be excited upon visible light excitation. The spectra reported in Figure 4 display a single, broad peak centered at ca. 550 nm echoing that of the EVOH parent component. As TiO₂ is an indirect band gap semiconductor, band-edge luminescence is very difficult to observe because of the low emission probabilities of indirect transitions.^{15–17,47} This means that the dominance of the EVOH component in the photoluminescence spectrum is by no means a surprise. The analysis of the intensity of the organic-like transition is nevertheless rather informative. As can be seen in Figure 5 (top), a growth of the PL intensity

is observed for samples having oxide content up to 0.50 wt. %, while the intensity underwent a strong decay afterward. x TiAg films having an inorganic content above 2 wt. % display lower PL intensity than the EVOH single component. This behavior essentially mimics the one described for the x Ti reference nanocomposite films.²⁵ The whole intensity behavior shows the existence of energy/charge transfer(s) through the polymer/oxide interface, demonstrating again the intimate contact between these two components. For samples with nanoparticle content around/above 2 wt. %, the strong decay of the signal would indicate, according to the band gap and position of the components, a potential exciton (from the organic component) and/or hole (from the inorganic component) transfer(s), followed by an efficient charge (electron and hole) separation, leaving in this way holes into organic-like electronic states while electron could be preferentially located into inorganic-like states.^{47–49} As a final effect, such charge carriers can reach the surface of the nanocomposite materials and would be efficiently involved in the photokilling of microorganisms (see below).

The PL signal observed under visible light excitation gives some clues that allow a definitive interpretation of the visible absorption features appearing in the corresponding spectra of the nanocomposite films (Figure 3). As mentioned above, a growing light-scattering phenomenon (with the inorganic component content) may be envisaged to contribute to the strong UV-A and visible absorption increase observed for the x TiAg samples in Figure 3 with respect to the parent EVOH–TiO₂ systems; however, the PL intensity shown in Figure 5 (bottom) provides conclusive evidence for the presence of true, electronic states in the visible region of the electromagnetic spectrum. In the case of x Ti reference nanocomposites (open symbols in Figure 5), it appears that these new states, unequivocally ascribable to the nanocomposite system and absent in the parent (EVOH, TiO₂) monocomponent systems, suffer a strong charge recombination upon de-excitation for 0.5Ti to 1Ti films, moderating this behavior for 2Ti and 5Ti samples. The presence of Ag in the nanocomposite films triggers, however, a significantly different behavior as a function of the inorganic content of the material. Besides notably decreasing the intensity (see the 0.3 factor in Figure 5 bottom) with respect to the x Ti series, we observed a trend recalling that displayed under pure UV light. In essence, this indicates a fundamental difference between the x TiAg and x Ti systems upon visible-light excitation, related, in turn, to the different nature of the electronic states involved. This clearly points out the key role played by the silver LSP resonance. It is obvious that upon excitation the main absorption process takes place on silver and electrons would remain at the inorganic nanoparticles while holes would be mostly handled by the organic component, favoring their presence at the surface of the material. In brief, the presence of this absorption band allows the adequate handling of the charge carriers and, by analogy to the already discussed UV case, an enhancement of the charge separation and subsequent involvement of these species on biocidal steps. Interesting to note is the essential constancy of the PL behavior upon visible-light excitation for the x TiAg systems before/after contact with the microorganisms (Figure S2, Supporting Information), indicating the stability of the organic–inorganic interface. This is indirect evidence suggesting that the metal state of silver remains stable throughout the biocidal tests. Overall, the optical characterization of these materials shows that they act as a biocidal agent as a whole; this changes the character of the biocidal inorganic component from that of a contact agent to a noncontact one and helps in the work of destroying microorganisms, as the

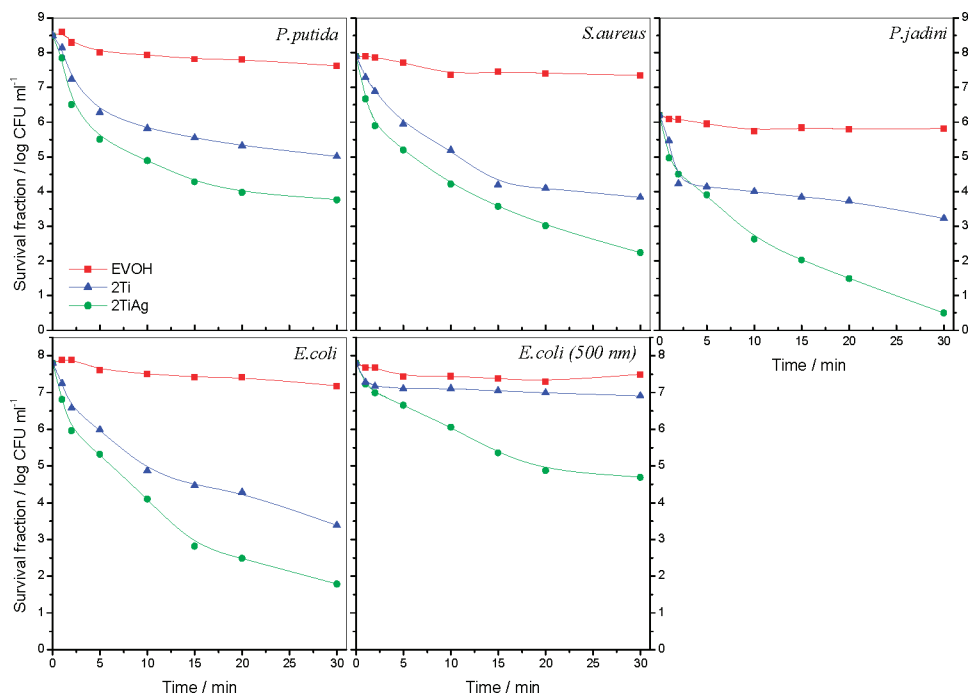


Figure 6. Process come-up time logarithmic reduction of the microorganism population suspended in the appropriate liquid media according to the microorganisms tested. Survival curves for four microorganisms as a function of the irradiation time for 2TiAg, 2Ti, and EVOH-control samples.

complete surface of the nanocomposite becomes biocidal upon both UV and visible-light excitation. Note also that EPR tests using oxygen as probe molecule (result not shown) did not detect the presence of the inorganic component at the surface. Leaching tests confirmed such results and indicate the null toxicity of the nanocomposite systems.

Kinetics of antimicrobial activity of the different x TiAg and 2Ti and EVOH reference materials toward two Gram-negative bacteria (*E. coli* 1337-H and *P. putida* KT2440), a Gram-positive cocci (*Staphylococcus aureus* 1341-HT), and a yeast (*Pichia jadini* CECT 1062) were investigated. In these experiments, rather limited, sublethal energy fluences of ca. 1 kJ m^{-2} were employed. The relatively innocuousness of the UV/visible radiation(s) is (are) demonstrated by the blank experiments in presence of the EVOH matrix; a maximum of ca. 1 log CFU-reduction (CFU: colony forming unit) is observed in our tests (Figure 6), in accordance with previous results.^{21,22,24,25} The 2Ti sample was previously tested with three of these cultures and gives optimum performance with respect to the inorganic content of the material.²⁵ Figure 6 shows the 2Ti and 2TiAg film performance while the behavior of the x TiAg series as a function of the inorganic content is plotted in Figure S3, Supporting Information. The comparison of the x TiAg materials with the 2Ti nanocomposite gives the result expected from the optical characterization, an overall enhancement of the antimicrobial activity, particularly acute for loadings above 2 wt %. Upon UV excitation, we obtain the best results for 2TiAg in all cases, although 5TiAg showed similar performance in the killing of the yeast *Pichia jadini*. As previously discussed for the x Ti series, the behavior of the x TiAg series indicates a trade off between the available oxide surface area and the enhanced photoactivity displayed for samples with a inorganic content above 2 wt % and induced by an optimized charge carrier separation as deduced from PL measurements.²⁵ The inorganic component dispersion starts to decay for the 5TiAg sample and would thus justify that the optimum activity is obtained for films with an oxide content in the 2–5 wt % range. Interestingly,

the high antimicrobial performance of the x TiAg films is maintained upon visible-light excitation (500 nm), showing an outstanding 3/4 maximum log-reduction for 2TiAg/5TiAg samples. This contrasts with the modest (and predicted) performance of the 2Ti film. As Figure 6 experiments with *E. coli* demonstrated, Ag-containing materials are thus well suited to work under visible light and, therefore, to extend with rather high efficiency the action of TiO₂-based biocides to this part of the electromagnetic spectrum.

The biocidal tests demonstrate that irrespective of the excitation wavelength the x TiAg nanocomposites show up at least ca. 4–5 log-reduction (e.g., 99.99–99.999% killing), a biocidal level particularly significant upon visible-light excitation (see below). This killing level is commonly understood as being bactericidal and, as detailed elsewhere, is sufficient to maintain a good (human health) safety control, helping to eliminate the need for sterilization or other aggressive treatments of foods.⁵⁰ Comparison with previous results concerning the efficiency of inorganic/organic biocidal agents is easy in the case of *E. coli*^{51–58} and *S. aureus*.^{59,60} There is also a significant number of studies devoted to both pathogens,^{61–68} but the control of *P. putida* has been only pursued using chemical agents⁶⁹ while, to our knowledge, only our previous work has considered the killing of *P. jadini*.²⁵ Although antimicrobial tests are strongly dependent on the specific experimental conditions used, for a simple comparison we can indicate that our maximum log reduction, ca. 5.5/5.6, attained after 0.5 h for, respectively, *E. coli*/*S. aureus*, can be compared with previous results on *E. coli* using TiO₂–polymer nanocomposite films, with ca. 5.4/6.3/1 log-reduction for, respectively, 1.5/1/1 h (s) of treatment.^{56,63,64} Moreover, it is interesting to stress that previous results using visible light for TiO₂–polymer films give relatively low (40%/1 h) deactivation performance against *E. coli*, far from that presented here.⁵⁷ Similarly, ca. 0.8/1 log-reductions were reported after, respectively, 0.5/12 h of treatment in the case of *S. aureus*.^{61–66} The killing action of x TiAg films also compares favorably with Ag–polymer (PEO; polyethylene oxide) or

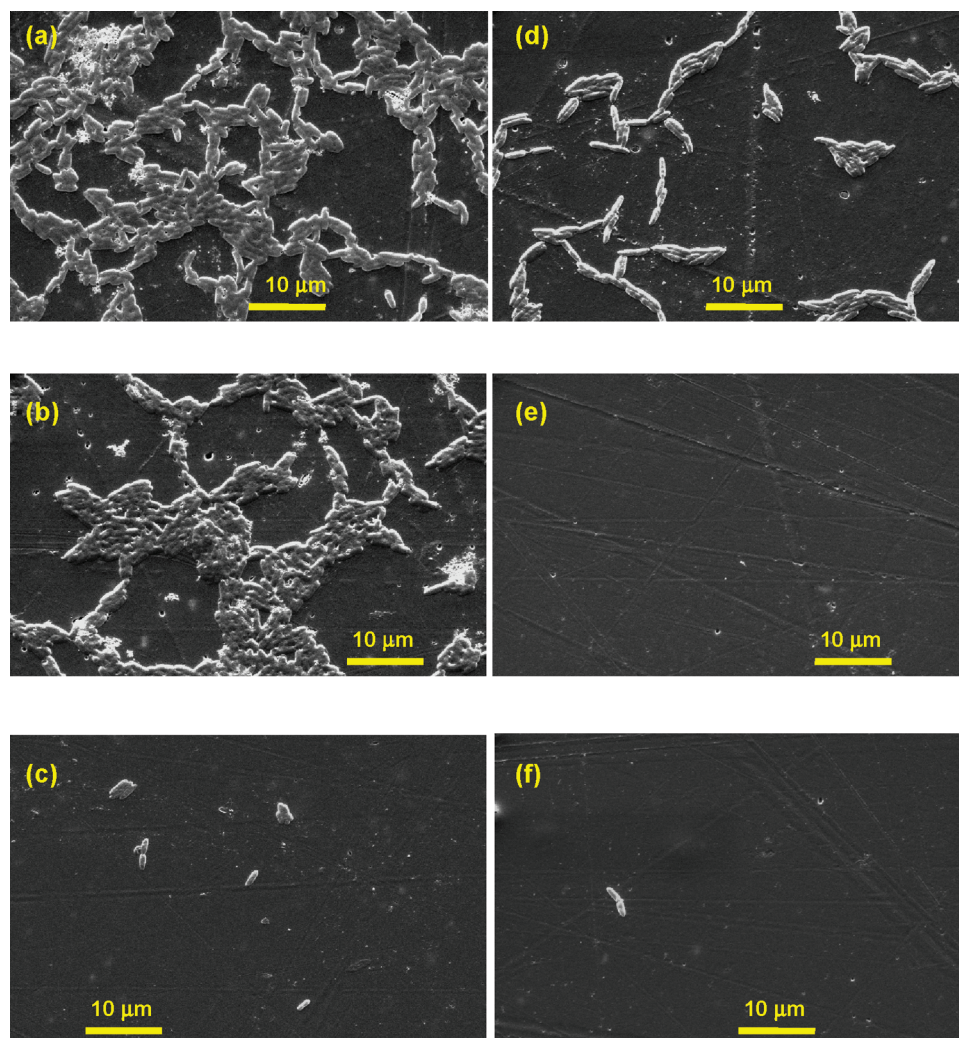


Figure 7. SEM images of the *P. putida* cells positioned at the surface of the *x*TiAg nanocomposites in the presence and absence of UV light: (a) Survey view of biofilm adhesive growth of cells on an EVOH substratum but irradiated with UV (substratum control). (b) UV control, i.e., cells grown in the presence of 2TiAg but without UV irradiation. (c) Cells grown after UV treatment in the presence of reference 2Ti. (d) Cells in the presence of 05TiAg and after UV irradiation. (e) After UV exposure in the presence of 2TiAg. (f) After UV exposure in the presence of 5TiAg.

antibiotic–apatite–EVOH films, which appear to require larger times (hours vs minutes) to obtain similar killing levels for both *E. coli/S. aureus*.^{68,70} In brief, comparison with measurements using TiO₂ powders,^{51,50,61,60} immobilized antibiotics on polymers (EVOH),⁶⁸ immobilized/supported TiO₂ on polymers (acetate, Plexiglas, polystyrene),^{53–55,63,63} Ag nanocomposites^{58,59,66,67,70} and also negative air ions generated with the help of electrical fields⁶⁰ supports the general conclusion concerning the excellence of the films presented here, regardless of the nature of the microorganism or the light source (UV, visible) characteristics.

A SEM study of *P. putida* adhesion and biofilm formation was performed to further analyze the bactericidal properties of our nanocomposites and to translate the data depicted in Figure 6 and Figure S3 in visual information. The genus *Pseudomonas* constitutes a large diverse group of ubiquitous, mostly saprophytic bacteria that inhabit soil, water, plants, and animals (including humans) and are well-known for their broad metabolic versatility and genetic plasticity.⁷¹ Among them, *P. putida* KT2440 constitutes a cosmopolitan opportunist par excellence because of its ability to protect from external factors by forming biofilms on most surfaces, including biliary stent.²⁷ As can be observed in Figure 7, adhesion/interaction of this bacteria to/with the polymer surface is certainly modified by UV light and/or by

the presence of TiO₂. In the absence of the oxide but under actual UV treatment, cells appear mainly aggregated by lateral contact of two or more cells. In the presence of 2 wt % Ag–TiO₂ but without UV irradiation, a similar aggregation state is encountered. Numerical analysis of the biofilm bacterial densities (given as number of cells per square millimeter) is presented in Figure 8. This indicates that the UV treatment has a relatively limited influence on cell viability, in agreement with results reported in Figure 6. Illumination of the TiAg nanocomposite systems using similar experimental conditions as in Figure 6 makes, as expected, a dramatic effect on cell viability. While a significant decrease in survival probability is detected for the 0.5 wt % composite, a complete or near-complete killing is observed for the other two composites having larger Ag–TiO₂ loadings (Figures 6 and 7). Differences between *x*Ti and *x*TiAg nanocomposites are already visible from the smaller inorganic content used (0.5 wt %), again reinforcing the idea that the silver LSP resonance plays a capital role on the biocidal behavior of the nanocomposite systems. Note, on the other hand, that the photokilling process does not produce significant amounts of flattened ghosts and similar bacterial residues. Because dead cells and debris provide an organic conditioning layer, the first step in biofilm formation,^{72,73} its absence allows an optimum

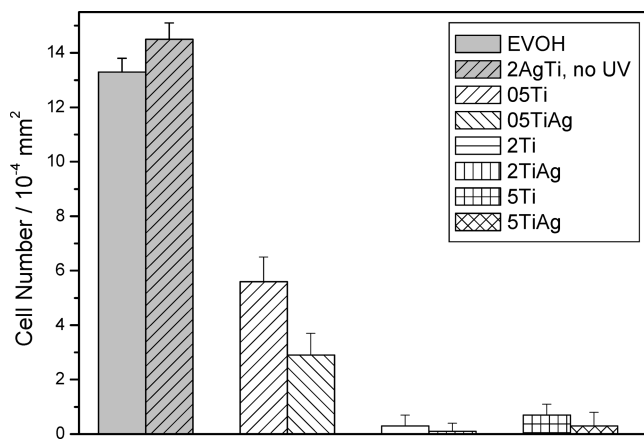


Figure 8. Impact of Ag-TiO₂ on *P. putida* cell number per mm² after treatment of the EVOH-control and xTi, and xTiAg nanocomposites in the presence and absence of UV light.

and continuous use of the nanocomposite material and limits a potential loss of efficiency by excessive accumulation of cellular debris at the surface. Thus, these data provide conclusive evidence that the presence of TiO₂ not only affects cell viability but also biofilm formation.

3. Conclusions

In summary, we have described a novel, highly efficient biocidal material composed of a mixed Ag-TiO₂ inorganic nanocomponent and an EVOH polymer commonly used in the industry. Through a plasmonic effect, the presence of minute amounts of silver significantly enhances the antimicrobial power of the known and similar TiO₂-EVOH systems under UV light and introduces the successful use of visible-light sources. The joint UV-vis and photoluminescence optical characterization of the films gives conclusive evidence of the plasmonic nature underneath the general enhancement of the biocidal properties observed with both UV and visible light. As discussed, this presumably occurs through the LSP resonance interaction with nanocomposite-related (e.g., states not associated individually with any of the inorganic/organic components) electronic states. The interaction not only optimizes the UV/visible photon handling (excitation/de-excitation) by the films but also makes the whole surface of the nanomaterial biocidal and eliminates the necessity of contact between the primary biocidal inorganic agent and the microorganisms.

The nanocomposites were capable of killing Gram-negative and positive bacteria/cocci and yeasts on surfaces and in solution with an outstanding killing performance (above 99.999% microorganism reduction in our experimental conditions), irrespective of the energy of the excitation light. Moreover, SEM analyses showed that xTiAg nanocomposite films inhibit biofilm formation. Overall, the antimicrobial properties showed an optimum for the 2TiAg nanocomposite. The potent antimicrobial action showed by the TiAg nanocomposites together with their null toxicity would indicate that such materials may find use for a wide variety of packaging, coatings for “clean surfaces”, and biomedical or general applications.

Acknowledgment. Financial support from CSIC and MEC is acknowledged by Dr. A. Kubacka and Ms. C. Serrano for their I3P postdoctoral and FPU predoctoral grants, respectively. This work was supported by the CSIC under projects PIF200580F0101 and PIF200570F103. M.F. acknowledges the support by the Spanish GEN2006-27750-C-4-E project. The synchrotron work was

supported by the European Community—Research Infrastructure Action under the FP6 “Structuring the European Research Area” Programme (through the Integrated Infrastructure Initiative “Integrating Activity on Synchrotron and Free Electron Laser Science”), contract RII3-CT-2004-506008 (IA-SFS). We thank the Hasylab personnel, especially Dr. S. S. Funari, for collaboration on the soft-condensed matter beamline A2.

Supporting Information Available: Data concerning SEM, photoluminescence, and photokilling experiments are presented in this section. This material is available free of charge via the Internet at <http://pubs.acs.org>.

References and Notes

- Appendini, P.; Hotchkiss, J. N. *Innovative Food. Sci. Technol.* **2002**, 3, 113–126.
- Devlieghere, F.; Vermeir, L.; Debevere, J. *Int. Dairy J.* **2004**, 14, 273–285.
- Brody, A. L. *Food Technol.* **2003**, 57, 52–54.
- Tang, H.; Doerksen, S.; Tew, G. N. *Chem. Commun.* **2005**, 12, 1537–153.
- Gilbert, B.; Markova, N.; Cossement, D.; Gouttebaron, R.; Jeromec, C. *Langmuir* **2006**, 22, 255–262.
- Brayner, R.; Ferrari-Iliou, R.; Brivois, N.; Djediat, S.; Benedetti, M. F.; Fievet, F. *Nano Lett.* **2006**, 6, 866–870.
- Sambhav, V.; Mecbridge, M.; Peterson, B. R.; Sen, A. *J. Am. Chem. Soc.* **2006**, 128, 9796–9808.
- Dizman, B.; Elasri, M. O.; Mathias, L. *Biomacromolecules* **2005**, 6, 514–520.
- Iconomopoulou, S. M.; Voyatzias, G. A. *J. Controlled Release* **2003**, 103, 451–464.
- Sagripanti, J. C.; Bonifacio, A. *J. AOAC Int.* **2000**, 83, 1415–1422.
- Chen, Y.; Worley, S. D.; Kim, J.; Wei, T. Y.; Santiago, J. I.; Williams, J. F.; Sun, G. *Ind. Eng. Chem. Res.* **2003**, 42, 280–284.
- Robbins, M. E.; Hopper, E. D.; Schoenfish, A. *Langmuir* **2004**, 20, 10296–10302.
- Klibanov, A. M. *J. Mater. Chem.* **2007**, 17, 2479–2482.
- Nohynek, G. J.; Lademann, J.; Ribaud, C.; Roberts, M. S. *Crit. Rev. Toxicol.* **2007**, 37, 251.
- Dietbol, U. *Surf. Sci. Rep.* **2003**, 48, 53.
- Fernández-García, M. A.; Martínez-Arias, A.; Hanson, J. C.; Rodríguez, J. A. *Chem. Rev.* **2004**, 104, 4063.
- Hoffmann, M. R.; Martin, S. T.; Choi, W.; Bahemann, D. W. *Chem. Rev.* **1995**, 95, 69.
- Carp, O.; Huisan, C. L.; Reller, A. *Prog. Solid State Chem.* **2004**, 32, 33.
- Gómez-Romero, P.; Sánchez, C. *Functional Hybrid Materials*; Wiley: New York, 2004.
- Sánchez, C.; Julián, B.; Belleville, P.; Popall, M. *J. Mater. Chem.* **2005**, 15, 3559–3592.
- Kubacka, A.; Serrano, C.; Ferrer, M.; Lundsford, H.; Bieleck, P.; Cerrada, M. L.; Fernández-García, M.; Fernández-García, M. *Nano Lett.* **2007**, 7, 2529–2534.
- Kubacka, A.; Cerrada, M. L.; Serrano, C.; Fernández-García, M.; Ferrer, M.; Fernández-García, M. *J. Nanosci. Nanotechnol.* **2008**, 8, 3241–3246.
- Awazu, K.; Fujimaki, M.; Rockstuhli, C.; Tominaga, J.; Murakami, H.; Ohki, Y.; Yoshida, N.; Watanabe, T. *J. Am. Chem. Soc.* **2008**, 130, 1676–1680.
- Kubacka, A.; Ferrer, M.; Martínez-Arias, A.; Fernández-García, M. *Appl. Catal., B* **2008**, 84, 87–93.
- Cerrada, M. L.; Serrano, C.; Sánchez-Chaves, M.; Fernández-Martín, F.; de Andrés, A.; Jiménez-Ribóo, R. J.; Kubacka, A.; Ferrer, M.; Fernández-García, M.; Fernández-García, M. *Adv. Funct. Mater.* **2008**, 18, 1949–1960.
- Food spoilage microorganisms*; edited by Blackburn Safety and Environmental Assurance Centre, Unilever, U.K.; Woodhead Publishing Limited: Cambridge; 2006; Chpt. 5.
- Nelson, K. E.; Weinel, C.; Paulsen, I. T.; Dodson, R. J.; Hilbert, H.; dos Santos, M.; et al. *Environ. Microbiol.* **2002**, 4, 799–808.
- Fernández-García, M.; Wang, X.; Belver, C.; Hanson, J. C.; Rodríguez, J. A. *J. Phys. Chem. C* **2007**, 111, 674–682.
- Ramos, J. L.; Marques, S.; Timmis, K. N. *Annu. Rev. Microbiol.* **1997**, 51, 341–373.
- Sambrook, J.; Fritsch, E. F.; Maniatis, T. *Molecular Cloning: A Laboratory Manual*, 2nd ed.; Cold Spring Harbor Laboratory Press: Cold Spring Harbor, 1989.
- Jagger, J. *Photochem. Photobiol.* **1981**, 34, 761.

- (32) Nakamae, K.; Kameyama, M.; Matsumoto, T. *Polym. Eng. Sci.* **1979**, *19*, 572–577.
- (33) Cerrada, M. L.; Pérez, E.; Pereña, J. M.; Benavente, R. *Macromolecules* **1998**, *31*, 2559–2564.
- (34) Matyi, R. J.; Schartz, L. H.; Butt, J. B. *Catal. Rev.* **1987**, *29*, 41.
- (35) García-López, D.; Picazo, O.; Marino, J. C.; Pastor, J. M. *Eur. Polym. J.* **2003**, *39*, 945–950.
- (36) Castrillo, P. D.; Olmos, D.; Amador, D. R.; González-Benito, J. *J. Colloid Interface Sci.* **2007**, *308*, 318–322.
- (37) Vladimirov, V.; Betcher, C.; Vassilou, A.; Papageorgiou, A.; Bikaris, J. *Compos. Sci. Technol.* **2006**, *66*, 2935–2942.
- (38) Wang, Z.; Li, G.; Pen, H.; Zhang, Z.; Wang, X. *J. Mater. Sci.* **2005**, *40*, 6433–6438.
- (39) Ma, D.; Akpalu, Y. A.; Li, Y.; Siegel, R. W.; Schadler, L. S. *J. Polym. Sci., Part B: Polym. Phys.* **2005**, *43*, 488–495.
- (40) Ash, B. J.; Siegel, R. B.; Schadler, L. S. *Macromolecules* **2004**, *37*, 1358–1365.
- (41) Reymaud, E.; Jonen, T.; Gautier, C.; Vigier, G.; Varlet, J. *Polymer* **2001**, *42*, 8759.
- (42) Zhang, H.; Wang, G.; Chen, D.; Lu, X.; Li, J. *Chem. Mater.* **2008**, *20*, 6543.
- (43) Lee, K.-C.; Lin, S.; Tsai, C.-S.; Lu, Y.-J. *Surf. Coat. Technol.* **2008**, *202*, 5339.
- (44) Ambid, M.; Teyssedre, G.; Mary, D.; Laurent, C.; Montanari, G. C. *IEEJ Trans. Fund. Mater.* **2006**, *126*, 1097.
- (45) Morlat-Therias, S.; Mailhot, B.; Gonzales, D.; Gardette, J. L. *Chem. Mater.* **2004**, *16*, 377–385.
- (46) Ambid, M.; Teyssedre, G.; Mary, D.; Laurent, C.; Montanari, G. C. *IEEJ Trans. Fund. Mater.* **2006**, *126*, 1097–1101.
- (47) Pen, D.; Zhao, N.; Wang, Q.; Jiang, S.; Ji, X.; An, L. *Adv. Mater.* **2005**, *17*, 1991–1995.
- (48) Greedham, N. C.; Peng, X.; Alivisatos, A. P. *Phys. Rev. B* **1996**, *54*, 17628–17637.
- (49) Scully, S. R.; McGehee, M. D. *J. Appl. Phys.* **2006**, *100*, 034907.
- (50) Gundermann; K. O.; Ruden, H.; Sunntag; H. G. *Liehrbuch der hygiene*; G. Fischer Verlag: Stuttgart, 1991.
- (51) Huang, Z.; Maness, P. C.; Blake, D. M.; Wolfrum, E. J.; Smolinski, S. L.; Jacoby, W. A. *J. Photochem. Photobiol. A* **2000**, *130*, 163–169.
- (52) Ibañez, J. A.; Litter, M. I.; Pizarro, R. A. *J. Photochem. Photobiol. A* **2003**, *157*, 81–85.
- (53) Robertson, J. M. C.; Robertson, P. K.; Lawton, L. A. *J. Photochem. Photobiol. A* **2003**, *175*, 51–56.
- (54) Cho, M.; Chung, H.; Choi, W.; Yoon, J. *Water Res.* **2004**, *38*, 1069–1077.
- (55) Joo, J.; Kwon, S. G.; Yu, T.; Cho, M.; Lee, J.; Yoon, J.; Hyeon, T. *J. Phys. Chem. B* **2005**, *109*, 15297–15302.
- (56) Lonnén, J.; Kilvington, S.; Al-Touati, F.; McGuigan, K. G. *Water Res.* **2005**, *39*, 877–883.
- (57) Zhang, X.; Su, H.; Zhao, Y.; Tau, T. *J. Photochem. Photobiol. A* **2008**, *199*, 123–129.
- (58) You, K.-Y.; Byeon, J. H.; Park, J.-H.; Hwang, J. *Sci. Total Environ.* **2007**, *373*, 572–575.
- (59) Ho, C.; Tobis, J.; Sprich, C.; Thomann, R.; Tiller, J. C. *Adv. Mater.* **2004**, *16*, 957–961.
- (60) Arnol, J. W.; Boothe, D. H.; Mitatell, B. W. *J. Appl. Poult. Res.* **2004**, *13*, 200–206.
- (61) Seven, O.; Dinder, B.; Aydemir, S.; Metin, D.; Ozinel, M. A.; Icli, S. *J. Photochem. Photobiol. A* **2004**, *165*, 103–107.
- (62) Mitoraj, D.; Janczyk, A.; Strus, M.; Kirsh, H.; Stochel, G.; Heczko, P. B.; Macyk, W. *Photochem. Photobiol. Sci.* **2007**, *6*, 642–648.
- (63) Kuhn, K. P.; Chaberny, I. F.; Massholder, K.; Stickler, M.; Benz, V. W.; Sonnag, H.-G.; Erdinger, L. *Chemosphere* **2003**, *53*, 71–77.
- (64) Wang, Z.; Li, G.; Peng, H.; Zhang, Z.; Wang, X. *J. Mater. Sci.* **2005**, *40*, 6433–6438.
- (65) Page, K.; Palgrave, R. G.; Parkin, P.; Wilson, M.; Sarin, S. L. P.; Chadwick, A. V. *J. Mater. Sci.* **2007**, *17*, 95–104.
- (66) Vohra, A.; Goswami, D. Y.; Deshpande, D. A.; Block, S. S. *Appl. Catal., B* **2006**, *65*, 57–65.
- (67) Cowan, M. M.; Abshire, K. Z.; Houk, S. L.; Evans, S. M. *J. Ind. Microbiol. Biotechnol.* **2003**, *30*, 102–106.
- (68) Oyama, A.; Yokoyama, Y.; Uchida, M.; Ito, A. *Biomaterials* **2006**, *27*, 3295–3305.
- (69) Dosti, B.; Guzel-Seydim, Z.; Greene, A. K. *Int. J. Dairy Technol.* **2005**, *58*, 19–24.
- (70) Chen, Q.; Yue, L.; Xie, F.; Zhou, M.; Fu, Y.; Zhang, Y.; Weng, J. *J. Phys. Chem. C* **2008**, *112*, 10004.
- (71) Clarke, P. H. The metabolic versatility of pseudomonads. *Antonie Van Leeuwenhoek* **1982**, *48*, 105–130.
- (72) La Motta, E. J.; Hickey, R. F.; Buydos, J. F. *J. Environ. Eng. Dev.* **1982**, *108*, 1326–1341.
- (73) Beech, I. B.; Gubner, R.; Zinkevich, V.; Hanjangsit, L.; Avci, R. *Biofouling* **2000**, *16*, 93–104.

JP901337E